Chapter 12
Superparamagnetic Iron Oxide Nanoparticles for Cancer Theranostic Applications

Dipak Maity, Ganeshlenin Kandasamy, and Atul Sudame

Abstract In the last few decades, superparamagnetic iron oxide nanoparticles (SPIONs—particularly magnetite (Fe_3O_4)/maghemite (Fe_2O_3) nanoparticles) have gained a great deal of attention in many biomedical applications, including magnetic targeting based cell isolation/sorting, tissue engineering, gene delivery, and magnetofection, due to their unique magnetic properties, excellent chemical stability, biodegradability, and low toxicity as compared to other magnetic materials (for instance, Co, Mn, and Ni). But recently, SPIONs (in the form of ferrofluids—i.e., SPIONs dispersed in a carrier fluid) have become a highly promising candidate for their use as therapeutic and diagnostic (theranostic) agents in cancer treatment applications such as magnetic fluid hyperthermia (MFH) and magnetic resonance imaging (MRI), respectively. However, the theranostic efficacies of the SPIONs (or ferrofluids) might alter due to the differences in their physicochemical/dispersibility/magnetic properties that are significantly impacted by their synthesis methods and their stabilization process. In this chapter, we have initially discussed the crystal structure/composition and different synthesis methods of the SPIONs. Then, we have described the role of the SPIONs in the formation of the ferrofluids along with their stabilization process via diverse interactions. Finally, we have discussed about their (1) intrinsic cancer theranostic applications of SPIONs such as magnetic fluid hyperthermia, magnetic resonance imaging, and magnetic nanoparticle-based drug delivery and (2) combined cancer theranostics applications including MRI as an adjuvant to fluorescence imaging, thermo-chemotherapy, thermo-radiotherapy, and thermo-immunotherapy.

D. Maity (✉)
Department of Chemical Engineering, Institute of Chemical Technology Mumbai, IOC Campus, Bhubaneswar, OD, India

G. Kandasamy
Department of Biomedical Engineering, Vel Tech Rangarajan Dr. Sagunthala R&D Institute of Science and Technology, Chennai, TN, India

A. Sudame
Department of Mechanical Engineering, Shiv Nadar University, Dadri, UP, India

M. Rai, B. Jamil (eds.), *Nanotheranostics*,
https://doi.org/10.1007/978-3-030-29768-8_12

Keywords SPIONs · Magnetic nanoparticles · Biomedical applications · Nanomedicine · Magnetic fluid hyperthermia · Magnetic resonance imaging · Ferrofluids · Theranostics · Cancer treatment

12.1 Introduction

Superparamagnetic iron oxide nanoparticles (SPIONs) are one of the most commonly used superparamagnetic nanoparticles (SPNs) and they are extensively investigated in various biomedical applications including drug delivery, magnetic fluid hyperthermia (MFH), magnetic resonance imaging (MRI), cell isolation and/or sorting, gene delivery, and tissue engineering due to their unique magnetic properties, excellent chemical stability, biodegradability, and low toxicity as compared to other magnetic materials (for instance, Co, Mn, and Ni) (Odenbach 2002; Prashant et al. 2010; Merbach et al. 2013; Wang et al. 2013; Demirer et al. 2015; Li et al. 2016; Ali et al. 2016). Generally, the SPIONs have core-shell structures which are composed of the magnetite (Fe_3O_4) and/or maghemite (γ-Fe_2O_3) cores, and the non-magnetic organic/inorganic surface coatings (or surfactants) (Kumar and Leuschner 2005; Maity and Agrawal 2007; Issa et al. 2013; Kandasamy and Maity 2015). The surfactants/surface coating molecules play an important role (along with the reactants during the synthesis process) in determining physicochemical properties (i.e., size, shape, surface charge, colloidal stability), and magnetic properties (magnetic susceptibility, saturation magnetization, superparamagnetic behavior) beside the purpose to protect the SPIONs from their aggregation/agglomeration. Moreover, the surface coating molecules enable them for effective surface functionalization or bio-conjugation (by bearing suitable surface functional groups), to improve biocompatibility (by reducing toxicity) and also to enhance hydrophilicity (water dispersibility) so that the SPIONs could be efficiently used for their instantaneous biomedical applications (Liu et al. 2009; Mahmoudi et al. 2011).

Iron oxide-based magnetic nanoparticles are usually synthesized in the nanodimensional regime—i.e., 1–100 nanometers (nm). In general, the large-sized magnetic particles display coercivity (H_c) and remanent magnetization (M_r) values due to their multi-domain structure ascribed to different crystallite orientations (as shown in Fig. 12.1). However, when the sizes of these particles are reduced to submicron (i.e., nanometer) regime, the multi-domain structure will get modified into a single-domain structure, and the coercivity value increases to maximum. The reduced nanometer-size at which these particles possess a single-domain structure is determined as single-domain size with a specific critical radius (r_c). For example, the r_c values of single-domain Fe_3O_4 and γ-Fe_2O_3 nanoparticles are, respectively, calculated as ~30 and ~60 nm (Trohidou 2014; Li et al. 2017). Also, when the size of the magnetic particles is reduced further, these particles might possess "super-

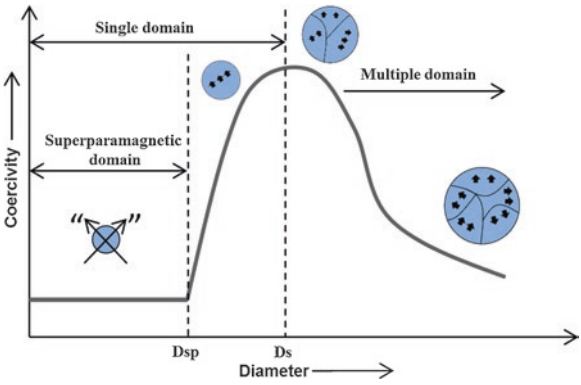

Fig. 12.1 Schematic representation of change in coercivity with the size of a magnetic nanoparticle)

paramagnetism" and this reduced size is called as superparamagnetic size, usually in the range of 4–20 nm for Fe_3O_4/γ-Fe_2O_3 nanoparticles at room temperature (Ortega and Giorgio 2012). Herein, "superparamagnetism" indicates that the size-reduced magnetic nanoparticles display a robust paramagnetic nature with high saturation magnetization (M_S) and magnetic susceptibility (χ) under the influence of an externally applied magnetic field. Moreover, these nanoparticles might lose their magnetization completely once the magnetic field is removed, which results in zero H_c and M_r.

Superparamagnetic iron oxide nanoparticles (SPIONs), especially magnetite (Fe_3O_4) nanoparticles, have an inverse spinal crystal structure composed of (1) both divalent iron (Fe^{2+}) and trivalent iron (Fe^{3+}) ions at octahedral sites and (2) one trivalent iron (Fe^{3+}) ions at the tetrahedral sites—as shown in Fig. 12.2 (Bastow and Trinchi 2009). Herein, the total stoichiometric ratio of Fe^{2+} to Fe^{3+} ions is 0.5. Moreover, the crystal structure of maghemite (Fe_2O_3) nanoparticles is similar to that of magnetite nanoparticles (i.e., spinel structure); however, the only difference is that all the iron ions are in the trivalent state (i.e., Fe^{3+} ions). Besides, the oxygen anions (O^{2-}) are arranged among the iron ions to form a close-packed array with cubic structure in both Fe_3O_4 and γ-Fe_2O_3 nanoparticles (Cornell and Schwertmann 2004; Qiao et al. 2009). Usually, the magnetic moments in the SPIONs (magnetite/maghemite) originate from the presence of unpaired 3d electrons in Fe^{3+}/Fe^{2+} cations in their crystal structure. However, these cations are located far apart from each other to hinder their interaction (for magnetic moment formation). Nevertheless, an exchange coupling between the cations (Fe^{3+} and Fe^{2+} ions) is possible through the non-magnetic oxygen anions (O^{2-}) which helps in the formation of the magnetic moments (Moskowitz 1991; Spaldin 2003; Tartaj et al. 2003; Liu et al. 2009; Thanh 2012; Wu et al. 2015).

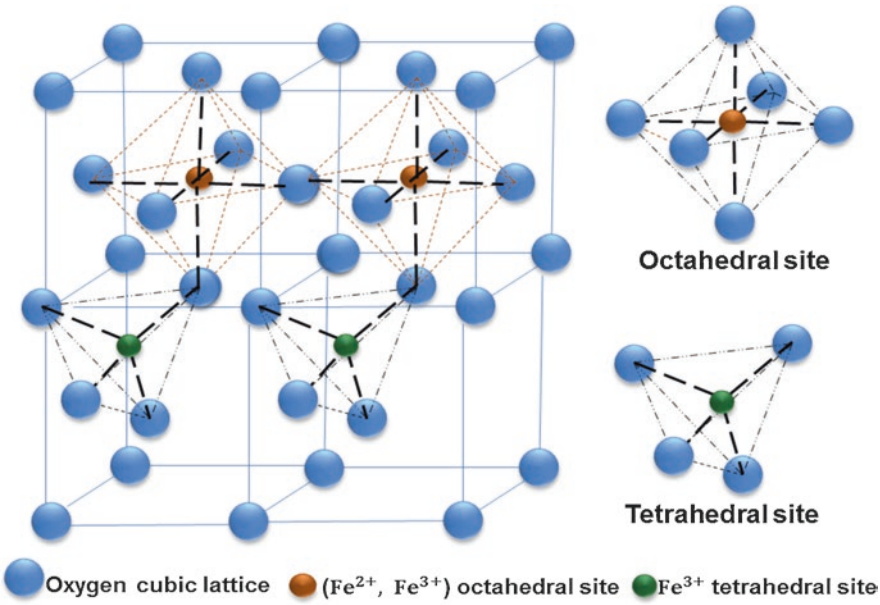

Fig. 12.2 Crystal structure representation of magnetite (Fe_3O_4) unit cell through ball-and-stick model. (Adapted from Bastow and Trinchi 2009)

12.2 Synthesis Methods

SPIONs are one of the common magnetic nanoparticles approved by Food and Drug Administration (FDA) for usage in biomedical applications such as cancer therapeutics and/or diagnostics (theranostics) (Revia and Zhang 2016; Stephen et al. 2012). However, in-depth studies are required to use these SPIONs effectively in theranostic applications under clinical scenarios. Therefore, the researchers are fine-tuning the synthesis methods to obtain high-quality SPIONs with good colloidal stability, high magnetization, and narrow size distribution. The following are the major hydrolytic and non-hydrolytic synthetic chemical routes that are widely utilized to synthesize high-quality SPIONs.

12.2.1 Hydrolytic Synthetic Routes

Hydrolytic synthetic routes are utilized as conventional routes to directly synthesize hydrophilic SPIONs, based on the chemical reactions among iron precursors in aqueous conditions. Besides, the SPIONs synthesized via hydrolytic methods are more appropriate for their instant biomedical applications. The major synthetic

routes including coprecipitation, hydrothermal, microemulsion, and sonochemical methods are discussed for the synthesis of SPIONs as follows.

12.2.1.1 Coprecipitation Method

Coprecipitation method is an extensively used hydrolytic route to synthesize SPIONs, where the precipitation of iron oxide nanoparticles is made via chemical reactions between ferric/ferrous salts (nitrates/sulfates/chlorides/perchlorates) and a base ($NaOH/NH_4OH$) under aqueous condition at slightly elevated temperatures (i.e., 40–80 °C). The main reaction mechanism involved in the formation of the SPIONs (for e.g., Fe_3O_4) is as follows (Ahn et al. 2012):

$$Fe^{2+} + 2Fe^{3+} + 8OH^- \leftrightarrows Fe(OH)_2 + 2Fe(OH)_3 \rightarrow Fe_3O_4 \downarrow + 4H_2O$$

This reaction is usually performed in an inert atmosphere (for e.g., nitrogen (N_2) or argon (Ar)) to avoid the formation of unwanted iron oxide phases (such as α-Fe_2O_3) in the as-synthesized SPIONs. Moreover, the reaction mechanism in the formation of the SPIONs usually passes through a topotactic transition (structural change to crystalline solid) phase in either one of the following routes: (1) nucleation → akaganeite phase → goethite → hematite/maghemite → magnetite (Fe_3O_4); (2) nucleation → ferrous hydroxide → lepidocrocite → maghemite → magnetite (Fe_3O_4). Furthermore, the path of this topotactic transition is majorly dependent on the variations in the pH of the aqueous reaction mixture. In addition, the physicochemical properties (such as shape, size, colloidal stability, and morphology) of the SPIONs can be tuned by altering reaction temperature, time of reaction, concentration of reactants, type of base, stabilizing agents, and reactant molarity (Mahmoudi et al. 2011; Ahn et al. 2012; Fu and Ravindra 2012; Mojica Pisciotti et al. 2014; Wu et al. 2015).

12.2.1.2 Microemulsion Method

Microemulsion is an optically transparent and thermodynamically stable solution and is classified into three major types: (1) water-in-oil, (2) oil-in-water, and (3) bicontinuous microemulsions. Out of these types, water-in-oil microemulsion is mostly used to synthesize the SPIONs, where the reverse micelles (containing the aqueous droplets of reactants—surrounded by a surfactant monolayer) are formed in a continuous oil phase, which might react with each other to form the SPIONs. Additionally, the synthesis of the SPIONs can also be carried out in either of the following two routes: (1) mixing of two or more microemulsions that contain different iron precursors; and (2) adding a precipitating agent (i.e., for example, ammonia) dropwise into the microemulsion containing the iron precursors. The reactions might take place inside the droplets (that mainly act as a nanoscale reactor) and the

final nanoparticles can be collected by removing the excessive surfactants/solvents (Boutonnet et al. 2008; Okoli et al. 2011). In this method, the physiochemical/magnetic properties of SPIONs are majorly dependent on the droplet size, concentration of the precursors, and type of surfactants/solvent.

12.2.1.3 Hydrothermal Method

Hydrothermal method is another conventional method used to synthesize the SPIONs (Kim et al. 2013). In this method, the nanoparticles are synthesized by performing the aqueous chemical reactions among the iron precursors in the presence/absence of the surfactants in a sealed container (inside an autoclave) which provide high temperature/vapor pressure (up to 250 °C/4 MPa) for chemical reactions. After the reaction, the mixture of aqueous solution is cooled down to the room temperature and the SPIONs are obtained by removing the residual surfactants, unreacted precursors, and other impurities. In this method, the physicochemical/magnetic properties of the SPIONs can be modified by tuning the reaction temperature, reaction time, amount of surfactant, and precursors (Kim et al. 2013; Piñeiro et al. 2015).

12.2.1.4 Sonochemical Method

Sonochemical method is based on inducing the reaction among mixture of iron precursors (for example, ferric or ferrous salts) via ultrasound irradiation having frequency ranging from 20 to 60 kHz to synthesize the SPIONs (Wu et al. 2008). This ultrasound irradiation (containing alternating expansive and compressive acoustic waves) generates cavitation microbubbles (i.e., cavities) in iron precursor solution, which induces nano-crystal nucleation by accumulating the ultrasonic energy. Finally, the microbubbles might collapse and subject to release the stored concentrated energy (with a heating and cooling rate of $>10^{10}$ K/s) that tends to increase the temperatures within the cavitation bubbles in a very short time (~1 ns) (Morel et al. 2008). Because of this, H^+ and OH^- radicals are produced through the decomposition of water, which further react with iron precursor mixtures to form the SPIONs (Yoffe et al. 2013). This method is beneficial to reduce unwanted growth of nano-crystals. However, the SPIONs with controlled physicochemical/magnetic properties are difficult to synthesize via this method (Pinkas et al. 2008; Wu et al. 2015).

Nonetheless, more research works are essential to overcome the drawbacks associated with these hydrolytic synthetic routes, including low crystallinity, broad particle size distribution, and/or complicated surface characteristics (Qiao et al. 2009).

12.2.2 Non-hydrolytic Synthetic Routes

The non-hydrolytic synthetic routes used in the preparation of the SPIONs are based on the chemical reactions of the iron precursors (in the presence/absence of surfactants) dissolved in organic solvents, which consequently results in hydrophobic SPIONs. Herein, thermal decomposition method is a major non-hydrolytic synthetic route used for the synthesis of the hydrophobic SPIONs with controlled physicochemical properties including size/shape/composition/crystal structure and magnetic properties (for instance, saturation magnetization) (Mutin and Vioux 2009; Qiao et al. 2009).

12.2.2.1 Thermal Decomposition Method

Thermal decomposition method (thermolysis) is based on the decomposition of the iron precursors (without/with the presence of surfactants) in high boiling point organic solvent by heating them at very high temperatures ranging from 200 to 350 °C. Herein, decomposition of the precursor occurs due to the breakage of their chemical bonds (via endothermic reaction) in an inert atmosphere by supplying continuous nitrogen/argon gas to avoid the formation of unnecessary iron oxide phases. The precursor materials and capping agents frequently used in the synthesis of the SPIONs via thermolysis are as follows: (1) iron precursors—ferric acetylacetonate ($[Fe(acac)_5]$ (acac = acetylacetonate)), iron pentacarbonyl ($Fe(CO)_5$), and iron cupferon ($[Fe(cup)_3]$ (cup = *N*-nitrosophenylhydroxylamine)); and (2) surfactants—oleylamine, hexadecylamine, oleic acid, linolenic acid, steric acid, and other fatty amines/acids (Demirer et al. 2015; Piñeiro et al. 2015). The physicochemical/magnetic properties of the SPIONs can be controlled by optimizing the reaction temperature, amount of precursors/surfactants, and reaction time (Maity et al. 2008).

Nevertheless, SPIONs prepared by this method are hydrophobic in nature, and cannot be directly used for cancer theranostic application. Therefore, the additional surface modification procedures like bilayer surfactant stabilization/ligand exchange methods are required to modify the hydrophobic nature of the surface of the SPIONs into hydrophilic nature. Recently, one-pot thermal decomposition method using polyol-based surfactants/solvents are extensively used to directly synthesize the hydrophilic SPIONs for instant use in cancer theranostic applications (Maity et al. 2008, 2009, 2010a, 2011a; Turcheniuk et al. 2013; Li et al. 2015; Piñeiro et al. 2015; Kandasamy et al. 2018a, 2019a, b).

12.3 Ferrofluids or Magnetic Fluids

12.3.1 Ferrofluid Formation: SPIONs as Building Blocks

Ferrofluids or magnetic fluids are homogeneous stable/colloidal suspensions of the SPIONs (coated with suitable molecules on their surfaces) that are dispersed in an appropriate carrier liquid (which can be polar/nonpolar). Hence, a typical ferrofluid or magnetic fluid consists of the following components (by volume): (1) magnetic solids (~5%), (2) surfactants (~10%), and (3) a carrier fluid (~85%) (Gupta and Gupta 2015). Moreover, the individual components that form the ferrofluids are explained as follows:

1. *Magnetic Solids*: Herein, the magnetic cores of the magnetic nanoparticles/solids act as a main source in the formation of the ferrofluids. The sizes of the magnetic cores inside the nanoparticles should be adequately (a) small enough for their uniform suspension in the carrier liquid via Brownian motion (which is the random motion of particles in a liquid due to multiple collisions among them) and (b) large enough to make considerable contribution in the magnetic response of the ferrofluids, while applying a magnetic field. Therefore, magnetic cores of the nanoparticles should have sizes $\leq D_{sp}$ or the individual nanoparticles should be superparamagnetic for their effective usage as magnetic solids. In general, SPIONs (such as Fe_3O_4 and/or γ-Fe_2O_3 nanoparticles) having sizes of 5–20 nm mainly act as the magnetic solids (Araki et al. 2009; Raj et al. 1995; Kalikmanov 2001).
2. *Surfactants*: The surfactants are mainly used to avoid clumping/aggregation and oxidation of the magnetic solids/SPIONs during the formation of the ferrofluids since (a) the SPIONs have very high dipole–dipole magnetic interactions and (b) it is difficult to maintain the dispersibility of the SPIONs in the ferrofluid suspensions by only Brownian motion—ascribed to their heavy weight (Raj and Boulton 1987). The surfactants mainly prevent the agglomeration/oxidation problems (even when exposed to the strong magnetic/gravitation fields and atmosphere) by creating strong electrostatic and/or steric repulsions around them. Generally, the surfactants consist of a polar head and/or a nonpolar tail (or vice versa), where one of their ends might adsorb onto the surface of the SPIONs and the other ends are exposed to the carrier liquid (to create repulsions) while forming ferrofluid suspensions. In addition, the surfactants play also important role in reducing the viscosity by decrementing the packing density of the SPIONs (Raj and Boulton 1987; Odenbach 2003; Scherer and Neto 2005; Gupta and Gupta 2015). The most commonly used surfactants in the ferrofluid formation are phosphonic acid, carboxylic acid, silane, catechol, polymers, and gold—as shown in Fig. 12.3 (Turcheniuk et al. 2013).
3. *Carrier Liquid*: The selection of a carrier liquid is significant in order to govern the overall physical properties of the ferrofluids. The carrier liquid is generally selected based on the following categories: (a) the surface nature (either hydro-

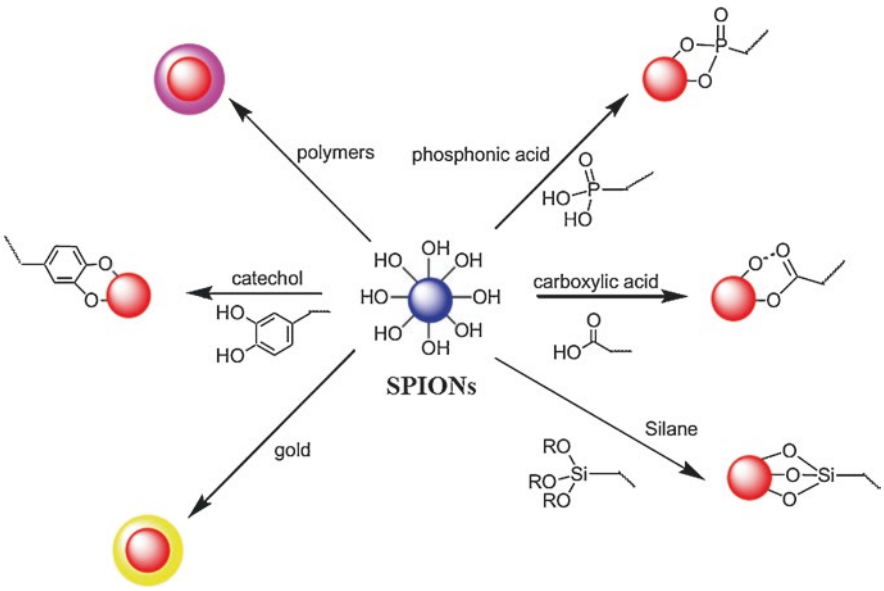

Fig. 12.3 Common surfactants used for the protection/stabilization of SPIONs. (Adapted from Turcheniuk et al. 2013)

phobic or hydrophilic) of the SPIONs, (b) field of application (water for biological applications), and compatibility of the SPIONs with the carrier liquid. The common carrier liquids (or solvent) used in ferrofluid formation include organic (hexane/toluene/tetrahydrofuran) or aqueous (water/biologic media including phosphate buffer saline (PBS), fetal bovine serum (FBS), and Dulbecco's modified eagle medium (DMEM)) based solvents (Raj and Boulton 1987; Raj et al. 1995; Odenbach 2003; Scherer and Neto 2005; Gupta and Gupta 2015).

12.3.2 Ferrofluid Stabilization

The stabilization of the ferrofluids is chiefly dependent on (1) the balance between the attractive and repulsive interactions, and (2) contribution from thermal energy. The typical nanoparticle diameter (D) to avoid the agglomeration can be evaluated by using the following equation that compares the thermal energy with the dipole–dipole pair energy.

$$D \leq \left(\frac{72 K_B T}{\pi u_0 M^2} \right)^{1/3}$$

where K_B, T, M, and u_0 are Boltzmann's constant, absolute temperature, intensity of magnetization, and permeability of free space, respectively. Moreover, it has been noted that the magnetic (i.e., dipole–dipole) interactions will be lower, if $D \leq 10$ nm.

12.3.2.1 Attractive Interactions

The two forces that are involved in the attractive interactions between the nanoparticles in the ferrofluid are (1) Van der Waals-London force and (2) magnetic dipole–dipole interaction force. Van der Waals-London force (U_{AW}) between two spherical particles—with a specific diameter (D) and separated by a limited distance (r)—is given by the following equation:

$$U_{AW} = -\frac{A}{6}\left[\frac{2}{\alpha^2-4}+\frac{2}{\alpha^2}+\ln\left(\frac{\left(\alpha^2-4\right)}{\alpha^2}\right)\right]$$

where $\alpha = 2r/D$ and A—Hamaker constant. Besides, Van der Waals force increases with the mass (size) of the nanoparticles. Moreover, the magnetic dipole–dipole interaction force (U_{Ad}) between two magnetic dipoles (μ_1) and (μ_2) separated by a specific distance (r) is given by the following equation:

$$U_{Ad} = -\frac{u_o}{4\pi^3}\left[u_1 \cdot u_2 - 3\left(u_1 \cdot \frac{\overline{r}}{r}\right)\left(u_1 \cdot \frac{\overline{r}}{r}\right)\right]$$

where $\overline{r}$ is the relative position of the nanoparticles. The total attractive force between two nanoparticles is the sum of their Van der Waals-London and magnetic dipole–dipole interaction forces.

12.3.2.2 Repulsive Interactions

The major two forces involved in the repulsive interactions between the nanoparticles inside the ferrofluid are (1) electrostatic repulsion (long range) and (2) steric repulsion (short range) forces. In ionic ferrofluids (i.e., the SPIONs are surface-coated with ionic surfactants), the electrostatic repulsive forces keep the nanoparticles apart to avoid their agglomeration for assuring the colloidal stability. Moreover, the electrostatic repulsive force (U_R) between two electrically charged spherical particles—with diameter (D) and separation by a distance (r)—is given by the following equation:

$$U_R = -\frac{D\pi\sigma^2}{\varepsilon_0\varepsilon_r k^2}\exp\left[-k\left(r-D\right)\right]$$

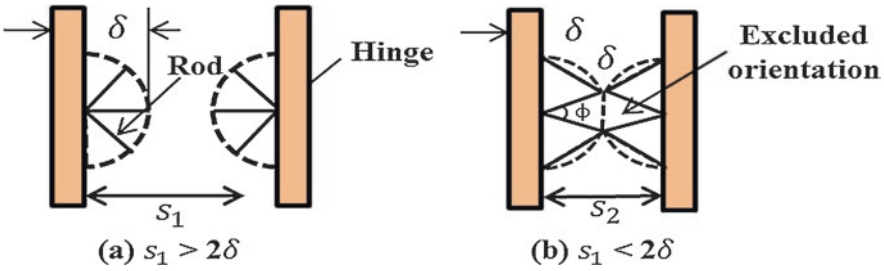

Fig. 12.4 Geometric illustration of steric repulsion energy using rigid rods attached onto universal hinge. (**a**) $s_1 > 2\delta$. (**b**) $s_1 < 2\delta$. (Adapted from Rosensweig 1997)

where σ is surface charge density and given by the equation: $\sigma = \varepsilon_0\varepsilon_r\varphi_0$ and ε ($\varepsilon_0\varepsilon_r$) is the electric permittivity of the fluid carrier. Moreover, φ_0 is surface potential of the charged nanoparticle at Helmholtz plane (in a double-layer model).

Besides, the steric repulsive force is linearly dependent on the temperature and can be understood by the geometric illustration of rigid rods attached onto a universal hinge—as shown in Fig. 12.4 (Rosensweig 1997). Here, the head pole groups of the surfactant are assumed to be adsorbed onto the surface, and the tail groups (rod) are assumed to form a specific hemisphere orientation under the thermal motion. The equation for the steric repulsive force between the spherical particles—having a specific diameter (D) with surfactants shell thickness (δ) and density (ξ molecular per nm^2), at temperature T—is given below:

$$\frac{U_t}{kT} = -\frac{\pi d^2 \xi}{2}\left[2 - \frac{l+2}{t}\ln\left(\frac{1+t}{1+l/2}\right) - \frac{l}{t}\right]$$

where $l = 2s/D$, and $s = r - D$ is the separation between the surfaces and $t = 2\delta/D$.

Thus, the colloidal stability of the nanoparticles in ferrofluid suspension is mainly dependent on the net content between the attractive and repulsive interactions among them. Moreover, the net interaction curve in the ferrofluid stabilization is given in Fig. 12.5 (Araki et al. 2009; Rosensweig 1997; Kalikmanov 2001; Scherer and Neto 2005).

12.4 Intrinsic Cancer Theranostic Applications

The most prominent cancer theranostic applications of the SPIONs include (1) magnetic fluid hyperthermia (MFH) therapy, (2) magnetic resonance imaging (MRI), and (3) magnetic drug delivery, where these SPIONs act as heating agents (HEA), contrast enhancing agents (CEA), and drug carriers, respectively (Kudr et al. 2017).

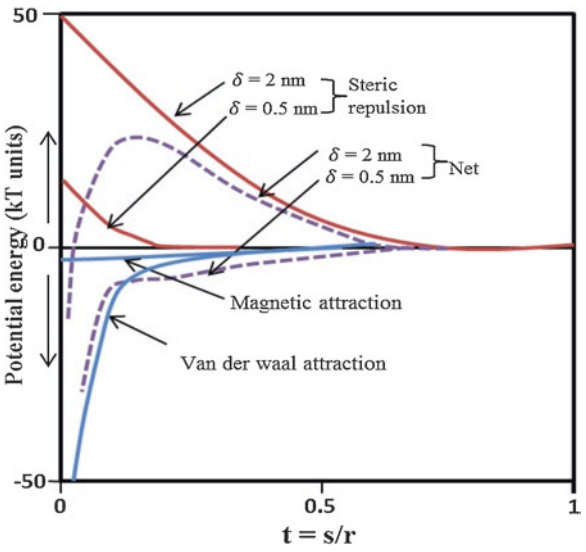

Fig. 12.5 The schematic curve represents the potential energy versus surface-to-surface separation of/distance between the colloidal stable SPIONs (with d = ~10 nm and molecular density of 10^{18} molecules). (Adapted from Rosensweig 1997)

12.4.1 Magnetic Fluid Hyperthermia Therapy

Magnetic fluid hyperthermia (MFH) therapy is a localized thermal therapy used for the treatment of malignant tumors/cancer, in which superparamagnetic nanoparticles (especially SPIONs) act as heating generating agents (Kandasamy and Maity 2015). Figure 12.6 gives a schematic representation of the application of the SPIONs (in the form of ferrofluids) in MFH application.

In brief, the SPIONs are normally delivered and localized near to the tumor site via passive/magnetic/active targeting, and subsequently exposed to an alternating magnetic field (AMF) for a certain time period (for e.g., ~1–2 h). This process generates heat which raises the tumor temperature to about 42–45 °C that is used for treating the cancer cells. Herein, the induced heat causes obstructions or ceases many cellular functions including cell proliferation and gene expressions in cancer cells which tends to induce cell death via apoptosis (Laurent et al. 2011; Revia and Zhang 2016). However, the heat produced during this therapy create very minimal damage to the nearby normal cells/organs as compared to other conventional treatment methods (for instance, chemo-radiation-therapies) (Hervault and Thanh 2014; Abadeer and Murphy 2016). Besides, the generated heat via this method could be controlled by tuning the physicochemical/magnetic properties of the SPIONs (including the size, shape, saturation magnetization, surfactants, and dispersion medium) and also the applied AMF (Kandasamy and Maity 2015; Kandasamy et al. 2018a, b).

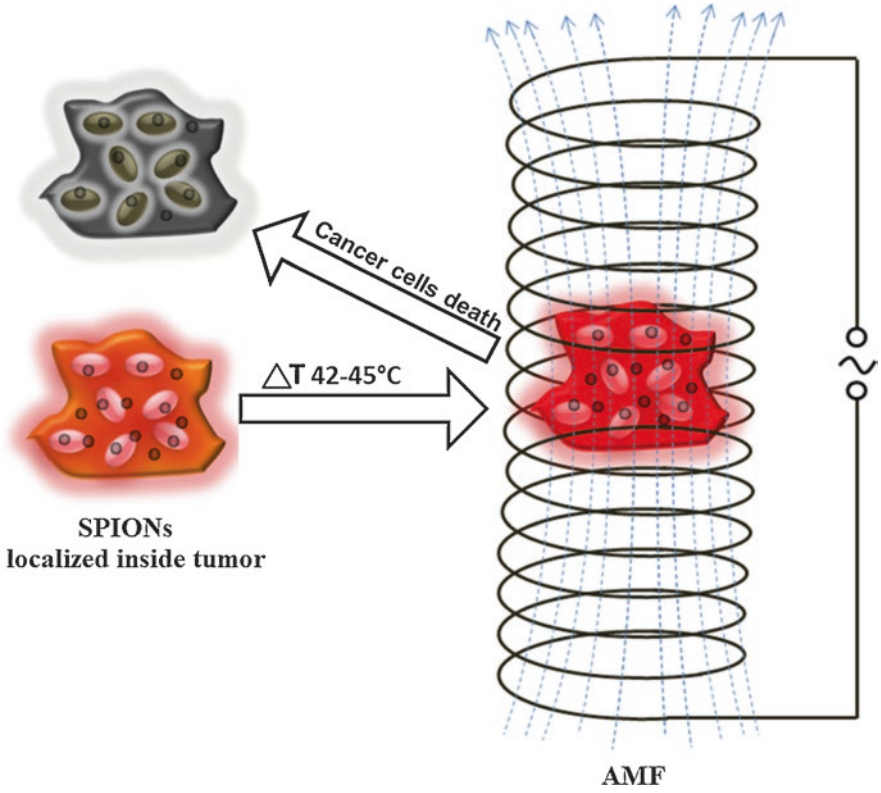

Fig. 12.6 Schematic representation of magnetic fluid hyperthermia (MFH) based cancer treatment by using ferrofluids containing the SPIONs

12.4.1.1 Heating Generation Mechanism

The heat generated by the SPIONs is due to the susceptibility loss, hysteresis loss, viscous heating or either one of their combinations, under the influence of the AMF. However, the susceptibility loss is a leading phenomenon for the heat generation in SPIONs, which majorly works on the Neel and Brownian relaxation losses. Generally, the magnetic moments of the SPIONs are fluctuated in the nanosecond timescale at their easy axis due to superparamagnetic nature (i.e., in the absence of an externally applied AMF). However, under the influence of an external AMF, Neel's relaxation time lag behind the reversal time of AMF (as shown in Fig. 12.7), which is caused by the energy of anisotropy that resists the magnetic moments to orient in the direction of applied AMF (Laurent et al. 2008). As a result, the energy that consumes to overcome the anisotropy is dissipated in the form of heat and known as "Neel relaxation loss." Moreover, the time for relaxation of magnetic moments of the nanoparticles (i.e., Neel relaxation time) is expressed by the following equation:

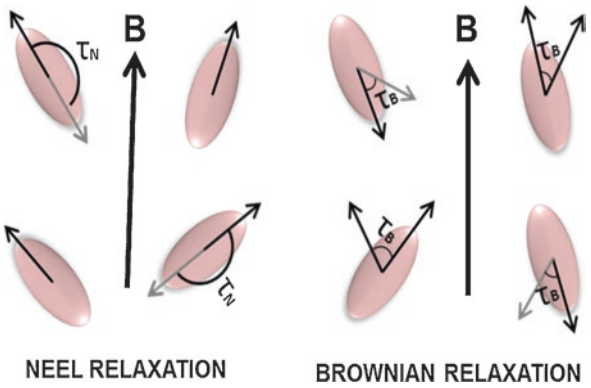

Fig. 12.7 Schematic representation of Néel and Brownian relaxation of SPIONs in colloidal suspension under the externally applied alternating magnetic field (AMF, marked as B)

$$\tau_N = \frac{1}{f_0}\exp\left[\frac{KV\left(1 - H/H_K\right)^2}{k_B T}\right]$$

where K, V, H, k_B, and T are the anisotropy constant (i.e., 3×10^5 ergs/cm^3 in the case of magnetite particles), volume of the nanoparticles, applied field, Boltzmann's constant, and measurement temperature, respectively. Moreover, f_0 is a constant with value 10^9 s^{-1}.

However, apart from Neel relaxation losses, the Brownian losses are also associated with the heat generation in SPIONs that originate from the hindrance to their physical rotational mobility (on application of an external AMF) by the viscosity of the carrier liquid (as shown in Fig. 12.7). Herein, the energy—that is consumed to overcome the viscosity—is dissipated in the form of heat. Moreover, the Brownian relaxation time is calculated by the following equation:

$$\tau_B = \frac{3VV_H\eta}{k_B T}$$

where V_H is the hydrodynamic volume of the SPIONs (by considering total effective diameter of the magnetic core and non-magnetic shell/coating), and η is viscosity of medium.

So the hindrances in the Néel and Brownian relaxations lead to a phase lag (between the AMF and the orientation direction of the magnetic moments/particles) that tends to generate heat in the form of susceptibility loss. Moreover, the heat induced by the SPIONs is also dependent on their size, shape, crystallinity, intrinsic magnetic properties, and the magnitude (H)/frequency (f) of the applied AMF. For instance, Néel and Brownian relaxations are dominant for the smaller and larger size SPIONs, respectively. Apart from susceptibility loss, other heating mechanisms such as hysteresis loss/viscous heating (stirring) are negligible for the SPIONs,

since they occur mainly in single/multi-domain magnetic particles (Bedanta and Kleemann 2009; Kozissnik et al. 2013; Laurent et al. 2011; Suto et al. 2009).

Moreover, the generated heat (i.e., heating efficacy) by the SPIONs is quantitatively determined in terms of specific absorption rate (SAR) which is expressed by the following relation (Kandasamy and Maity 2015; Lahiri et al. 2016).

$$SAR\left(\mathrm{W}/\mathrm{g}_{Fe}\right) = \frac{\rho_{\mathrm{samp}} \times C_{\mathrm{samp}}}{m_{Fe}} \frac{\Delta T}{\Delta t}$$

where ρ_{samp} and C_{samp} are, respectively, the solvent density and specific heat capacity. Moreover, m_{Fe} and $\Delta T/\Delta t$ are the weight fraction of the magnetic element (i.e., Fe) in the sample and initial slope of the time-dependent temperature curve, respectively. However, some researchers prefer to calculate the heating efficiency in terms of intrinsic loss power (ILP) via normalization of SAR by taking into account the AMF (frequency (*f*) and amplitude (*H*)) for better comparison of the reported results from different research laboratories. The ILP is calculated by the following equation (Lahiri et al. 2016).

$$ILP\left(nH\mathrm{m}^2/\mathrm{kg}\right) = \frac{SAR}{H^2 f}$$

12.4.1.2 SPIONs as Heating Agents

Initially in 1957, Gilchrist et al. have used the iron oxides nanoparticles (i.e., Fe_2O_3 nanoparticles with size of 20–100 nm) as heating agents for the lymph node treatment of dogs via MFH. This is performed by primarily injecting these nanoparticles into the lymphatic channels of dogs, and subsequently exposing the affected area to AMF for induction heating to destroy tumor cells (Gilchrist et al. 1957).

However lately, different research groups have performed various experimental investigations on the heat induction process of the SPIONs having various sizes, shapes, distributions, and organic/inorganic surface coatings under calorimetric/in vitro conditions to evaluate their potentiality for further in vivo applications or clinical trials. For instance, recently Maity et al. have synthesized triethylene glycol (TREG)/triethanolamine (TEA) coated magnetite (Fe_3O_4 with superparamagnetic character) nanoclusters and have performed the calorimetric studies under the applied AMF with H = 89 kA/m and f = 240 kHz, where these nanoclusters have shown SAR values in the range of 135–500 W/g. Moreover, 74% inhibition in the proliferation of MCF-7 cancerous cells is also attained (via MFH through these nanoclusters) when treated at a therapeutic temperature of 45 °C for 1 h (Maity et al. 2011b). Similarly, Gkanas has also demonstrated that TREG/decanethiol/polyethylene glycol (PEG-800)-coated SPIONs have induced considerable inhibition in the proliferation of three different cancer cell lines (DA3, MCF-7 and HeLa cancer) while applying the AMF with H = 26.48 kA/m and f = 765 kHz (Gkanas 2013).

Likewise, few in vivo MFH experiments in different cancerous animal models are also recently performed (by using SPIONs). For example, Rabias et al. (2010) have infused 150 μL of maghemite nanoparticles (10–12 nm) into the glioma tumors inside the rats, where MFH therapy is done for damaging the cancerous tissue by inducing a therapeutic temperature (for 20 min) under the applied AMF with $H = 11$ kA/m and $f = 150$ kHz (Rabias et al. 2010). In another MFH study, Ohno et al. have reported significant survival period for glioma-bearing rats while treated with carboxymethyl cellulose-coated SPIONs (for 10 nm) by applying the AMF with $H = 30.3$ kA/m and $f = 88.9$ kHz (Ohno et al. 2002). In similar fashion, arginyl glycylaspartic acid (RGD) peptide-conjugated and poly(maleic anhydride-alt-1-octadecene)-coated Fe_3O_4 nanoparticles have resulted in significant reduction in viability of liver cancers after MFH treatment on application of AMF with $H = 14$ kA/m and $f = 606$ kHz (Arriortua et al. 2016).

In addition, researchers have executed few clinical trials (at different phases (I/II/III)) by using MFH therapy for cancer treatment but with moderate achievements. However, very recently, researchers are majorly involved in (1) reducing the side effects associated with this MFH therapy and also (2) achieving high therapeutic efficacy by improving the inherent properties of SPIONs or by combining SPION-based MFH therapy with other therapies (Silva et al. 2011; Kitture et al. 2012; Thanh 2018).

12.4.2 Magnetic Resonance Imaging

Magnetic resonance imaging (MRI) is a diagnosis technique in radiology that uses the principles of radio waves, magnetism, and computer technology to produce anatomical images of human body. An MRI used with a nanoparticle-based contrast agent (for instance, SPIONs) is an effective way to detect the cancerous tumors located deep inside the body (Grover et al. 2015; Jo et al. 2016).

12.4.2.1 Relaxation Process

In general, the following process occurs in MRI: (1) initial alignment of nuclei (containing an odd number of protons and/or neutrons) in the direction of applied magnetic field; (2) then rotation of the aligned nuclei (also known as excitation) by applying a pulse of radio waves; and (3) finally emission of a radio signal by the nuclei while returning (also known as relaxation/realignment) to their equilibrium state, which is recorded by a radio-frequency (R.F.) detector (as shown in Fig. 12.8) and subsequently processed via a computer for images. In human MRI, the water molecules (especially hydrogen/proton nuclei) from different tissues are utilized to image the entire body in slices. Herein, the nuclei tend to excite and relax/realign (while applying the magnetic field/radio waves) at a specific time period, which is called as relaxation time that can be either T1 or T2 relaxation time ascribed, respec-

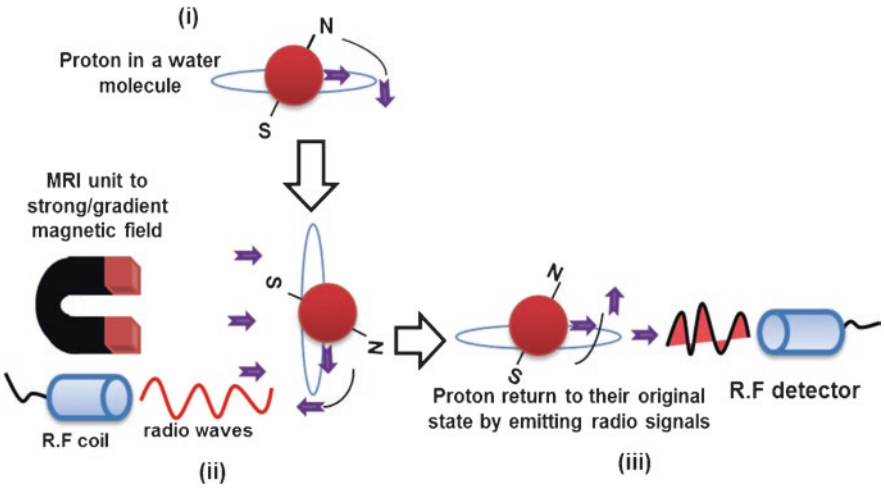

Fig. 12.8 Schematic representation of basic principle behind magnetic resonance imaging (MRI) based on hydrogen nuclei/proton excitation and relaxation

tively, to longitudinal (spin–lattice) or transverse (spin–spin) relaxations (Jacques et al. 2010; Stephen et al. 2012). Moreover, these relaxations differ diversely for various tissues which gives positive or negative contrast with corresponding relaxivity values of r1(1/T1) or r2(1/T2) (Nitz and Reimer 1999; Yin et al. 2004; Pooley 2005; McCarthy 2011).

12.4.2.2 SPIONs as Contrast Agents

Initially, the most widely used MRI contrast agents in clinical application are based on gadolinium (Gd(III)) complexes (used as positive contrast agent) including Magnevist® (Gadopentetic acid, Gd-DTPA—one of the oldest contrast agent approved by FDA in 1988), Multihance® (Gadobenate disodium, Gd-BOPTA), OptiMARK® (Gadoversetamide, Gd-DTPA-BMEA), and Omniscan® (Gadodiamide, Gd-DTPA-BMA). Nonetheless, various research investigations have raised concerns about the potential health risks (including nephrotoxicity) of these gadolinium-based complexes. Therefore, it is essential to find an alternative for gadolinium-based contrast agents for MRI imaging. Then recently, SPIONs are newly introduced as negative contrast agents for MRI applications since these nanoparticles tend to relax in transverse directions and they are more biocompatible/biodegradable and safe as compared to gadolinium complexes (Maity et al. 2010b; Tan et al. 2011; Corot and Warlin 2013; Chopra et al. 2016). Further, some of the SPION-based negative contrast agents are approved by FDA and in clinical trials also (Corot and Warlin 2013). In addition, very recently it has also been proved that the SPIONs having extremely small particle size (<5 nm) could potentially act as a positive contrast agent (Shen et al. 2017).

However, many researchers are widely involved in improving the relaxivity values of the SPIONs for providing better contrast and also to overcome the side effects associated with the usage of surfactants and concentration (Shen et al. 2017). For example, dextran-coated SPIONs (12 ± 2 nm) based negative contrast agents are prepared with high transverse relaxivity (r2) value of 90.5 ± 0.8 mM^{-1} s^{-1} at 7 T. Moreover, the in vivo MRI experiments in nude mice model have revealed that the as-prepared SPIONs are promising candidates for (1) tumor imaging, (2) specific organ imaging, and (3) whole body imaging at minimum concentration (i.e., 3 mg Fe/kg body weight) with negligible toxicity (Mishra et al. 2016). Similarly, maghemite (γ-Fe_2O_3) cores (with 13.08 ± 2.33 nm size) that are embedded inside a primary hydrophobic polymer (poly(4-vinyl pyridine), P4VP) matrix, and further covered by a shell of a secondary hydrophilic polymer (polyethylene glycol, PEG) are made, and have showed transverse relaxivity (r2) value of 104.7 ± 9.7 mM^{-1} s^{-1} at 4.7 T MRI and also negligible toxicity during in vivo study in liver of mice models (up to 30 days)—observed after the nanoparticle injection (Ali et al. 2017). In another study, nanometer-sized SPIONs (complexed with amylose nanoparticles that are cationized with spermine, ASP-SPIONs) labeled with transgenic green fluorescent protein (GFP)-mesenchymal stem cells (MSCs) were prepared for in vivo MRI tracking. Moreover, these SPIONs have exhibited a high transverse relaxivity (r2) value of 296.2 mM^{-1} s^{-1} in comparison to some commercially available SPION-based contrast agents such as Sinerem (~65 mM^{-1} s^{-1}), Endorem (120 mM^{-1} s^{-1}), and Resovist (180–202 mM^{-1} s^{-1}) (Lin et al. 2017). Recently, Wei et al. have developed zwitterion-coated ultra-small SPIONs—composed of ~3-nm-sized magnetic core and ~1-nm-sized hydrophilic shell—for use as positive contrast agents, which have displayed longitudinal (*r1*) relaxivity value of 5.2 mM^{-1} s^{-1} (at 1.5 T) that is slightly higher than the value of commercially available gadolinium-based positive contrast agent (i.e., 4.8 mM^{-1} s^{-1} at 1.5 T) (Wei et al. 2017). Despite the abovementioned improvements, SPION-based contrast agents are required to be crucially optimized in terms of better physicochemical (particle size/shape), water dispersibility, and magnetic (including relaxivities) properties for better clinical acceptance.

12.4.3 Magnetic Drug Delivery

Targeting techniques which are involved in the delivery of the chemotherapeutic drugs by using the SPIONs are classified as (1) passive targeting, (2) active targeting, (3) magnetic targeting, and (4) combined targeting (i.e., active + magnetic targeting). Passive targeting is based on the targeting of the drugs after their conjugation/encapsulation with SPIONs to the tumor sites through leaky vasculatures based on the enhanced permeability and retention (EPR) effect (Danhier et al. 2010; Kim et al. 2013; Xu and Sun 2013; Shin et al. 2015; Revia and Zhang 2016). However, passive targeting may be inadequate to achieve efficient targeting in the tumor sites, since it is solely relied on the EPR effect (Rosenblum et al. 2018). Therefore, active targeting of drugs is preferred over passive targeting to increase efficiency of their

delivery. The active targeting is achieved by the attachment/conjugation of targeting moieties (i.e., antibodies) and drugs onto the SPIONs for effective tumor antigen targeting based on ligand-receptor interactions (Hairston 1996; Prijic and Sersa 2011; Yu et al. 2012). Drug delivery is also performed by utilizing the SPIONs as a magnetic targeting agent to effectively deliver the chemotherapeutic drugs at the site of tumors for cancer treatment with/without the influence of an externally applied static magnetic field (Polyak and Friedman 2009; Laurent et al. 2014; Burgess et al. 2016; Zhu et al. 2017; Ansari et al. 2018). Moreover, MRI via SPIONs in real-time scenario can also be performed for simultaneous navigation, localization, and the release of the drugs at tumor sites to track their bioavailability (Kokura et al. 2016). Moreover, combined targeting involves active and magnetic targeting techniques, and a typical combined drug delivery system may consist of SPIONs, anticancer/chemotherapeutic drugs, targeting moieties (i.e., antibodies), and/or carriers (i.e., polymeric micelles/nanoparticles for encapsulation of SPIONs along with drugs) (Veiseh et al. 2011; Thomsen et al. 2015).

In a recent study, a multifunctional hybrid biocompatible nanoplatform (having a size of ~100 nm) has been prepared by constituting poly(lactic-co-glycolic acid) (PLGA) nanoparticles stabilized with chitosan and poly(vinyl alcohol) (PVA) and co-loaded with SPIONs and anticancer drug cisplatin (Ibarra et al. 2018). Then, they have confirmed that the as-prepared nanoplatform has been successfully internalized into both HeLa and MDA-MB-231 cells (determined through the cellular uptake studies) via passive targeting. In another recent study, antiCD44 antibodies and gemcitabine-conjugated multifunctional iron oxide nanoparticles were primarily developed, which have demonstrated the targeting (i.e., active targeting) of nanoparticles to different CD44-positive cancer cell lines using a CD44-negative non-tumorigenic cell line as a control to verify the specificity by ultrastructural characterization and downregulation of CD44 expression (Aires et al. 2016). Then, they have also showed the selective drug delivery potential of the nanoparticles by the killing of CD44-positive cancer cells using a CD44-negative non-tumorigenic cell line as a control. Herein, (1) CD44 is a lymphocyte homing receptor that has been overexpressed usually in a large variety of cancer cells, cancer stem cells (CSCs) and circulating tumor cells (CTCs), which is actively targeted via antiCD44 antibodies; and (2) gemcitabine is a chemotherapeutic drug—currently used for pancreatic cancer treatment in clinical scenarios.

Very recently, a 250-nm-sized nanocarrier system is prepared by constituting paclitaxel (a chemotherapeutic drug)/SPIONs co-loaded PEG-ylated PLGA-based nanoparticles (Ganipineni et al. 2018). An ex vivo bio-distribution study have showed an enhanced accumulation of the SPIONs in the brain of glioblastoma (GBM) bearing orthotopic U87MG mice with magnetic targeting. In addition, they have observed that the blood–brain barrier is disrupted in the GBM area via magnetic resonance imaging (MRI) studies, which confirms the entry of the SPIONs. Moreover, the magnetic targeting treatment based on these nanocarrier system have significantly prolonged the median survival time of GBM bearing mice models as compared with the passive targeting and control treatments, when tested for in vivo antitumor efficacy. In another investigation, multifunctional nanoparticles are pre-

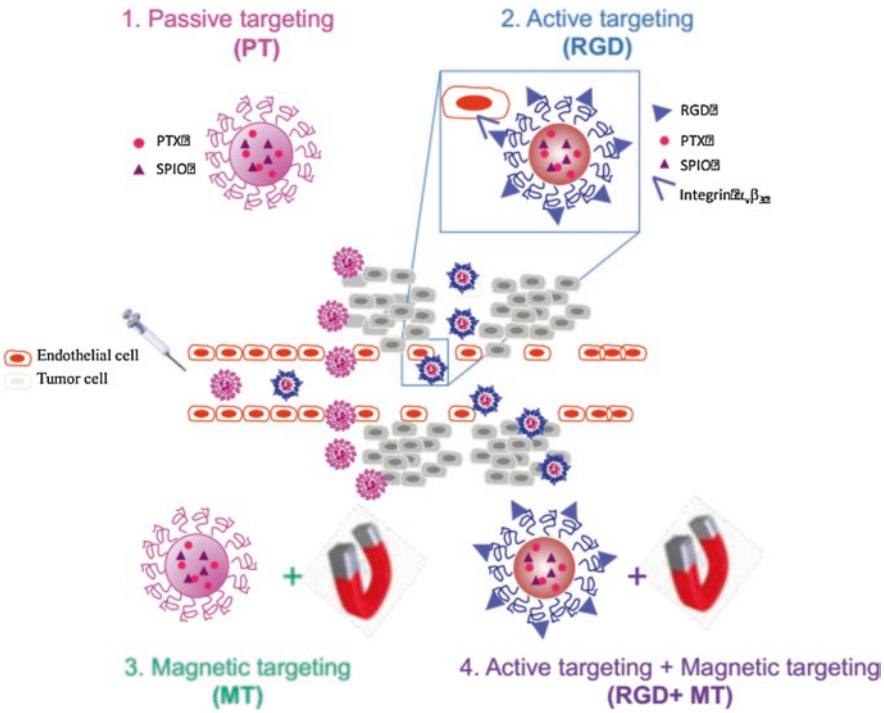

Fig. 12.9 Schematic representation of the different tumor targeting strategies. (1) *passive targeting* (PT) via the enhanced permeability and retention (EPR) effect, (2) *active targeting* of $\alpha_v\beta_3$ integrin via RGD grafting (RGD), (3) *magnetic targeting* (MT) via a magnet of 1.1 T placed on the tumor, and (4) the combination of the magnetic targeting and the active targeting of $\alpha_v\beta_3$ integrin (RGD + MT). (Adapted from Schleich et al. 2014)

pared by using PLGA-based nanoparticles loaded with paclitaxel and SPIONs and then compared through different in vivo targeting strategies: (1) passive targeting (PT) via the EPR effect, (2) active targeting of $\alpha_v\beta_3$ integrin via arginine–glycine–aspartic acid (RGD) grafting, (3) magnetic targeting (MT) via a magnet placed on the tumor, and (4) the combination of the active targeting of $\alpha_v\beta_3$ integrin and the magnetic targeting (i.e., RGD + MT)—as shown in Fig. 12.9 (Schleich et al. 2014). They have demonstrated that—as compared to non-targeted (i.e., PT) or single-targeted nanoparticles (i.e., RGD or MT)—the combination of both active and magnetic targeted strategies (i.e., RGD and MT) which have drastically enhanced (1) the nanoparticle accumulation into the tumor tissue with an eightfold increase as compared to passive targeting (1.12% and 0.135% of the injected dose, respectively), (2) contrast in MRI, and (3) anticancer efficacy with a median survival time of 22 days as compared to 13 days for the passive targeting. Finally, they have concluded that the double targeting of nanoparticles to tumors by different mechanisms could be a promising translational approach for the management of therapeutic treatment or personalized therapy.

12.5 Combined Cancer Theranostic Applications

The use of SPIONs is not only limited in their intrinsic cancer theranostic applications (as discussed above), but also for combined cancer theranostic applications to improve the effectiveness of cancer diagnosis and therapy. The combined cancer theranostics applications include: (1) MRI as adjuvant to fluorescence imaging, (2) thermo-chemotherapy (i.e., a combination of MFH therapy and chemotherapy), (3) thermo-radiotherapy (a combination of MFH therapy and radiotherapy), and (4) thermo-immunotherapy (a combination of MFH therapy and immunotherapy) (Zhang et al. 2013; Hervault and Thanh 2014; Mclaughlin et al. 2015; Grifantini et al. 2018), which are discussed below.

12.5.1 MRI as Adjuvant to Fluorescence Imaging

MRI is a significant diagnosis tool used for the detection and planning of cancer treatment. However, a single imaging technique is not adequate enough to examine multiple aspects of cancers due to the limitations in detection sensitivity, resolution, and specificity. In cancer treatment, accurate discrimination between the cancerous tissue from healthy tissue should be done during diagnosis to avoid severe damages to normal/surrounding tissues and effective treatment (Stephen et al. 2012; Mclaughlin et al. 2015). This could be achieved by utilizing a multimodal diagnostic approach (such as MRI as an adjuvant to fluorescence imaging) to enhance the spatial resolution and detection sensitivity in cellular imaging, which might be done by developing a multifunctional nanoparticle system by conjugating/co-encapsulating the SPIONs (for MRI) along with other fluorescence agents (for fluorescence imaging) such as fluorescence dyes (fluorophores, for example, Alexa Fluor 647/750) and quantum dots (QDs, for example—carbon QDs) (Josephson et al. 2002; Fass 2008; Maxwell et al. 2008; Kosaka et al. 2009; Ito et al. 2014; Wu et al. 2016).

Recently, multifunctional Fe_3O_4-gold (Au) hybrid nanoparticles are prepared by simultaneous conjugation of two fluorescent dyes or alternatively the combination of a drug and a dye, selectively binding to Fe_3O_4 and Au, which are as follows: (1) Fe_3O_4-Au nanoparticles functionalized with covalently attached Sulfo-Cyanine5 NHS ester derivative (Cy5) fluorescent dye via thiol-Au bonds for nanoparticle tracking; and (2) an anticancer drug doxorubicin (DOX) or Nile Red dye is loaded into the polymeric shell at the Fe_3O_4 surface (Efremova et al. 2018). The in vitro studies have revealed (1) high accumulation of fluorescent (Cy5) labeled Fe_3O_4-Au hybrids on 4T1 tumors (via passive targeting), (2) successful therapeutic payload (i.e., Dox) delivery and release to the tumors via Fe_3O_4-Au hybrids labeled with Cy5 and co-loaded with Nile Red dye, and (3) high diagnostic potential of Fe_3O_4-Au hybrids in 4T1 cells via MRI based on the enhanced relaxivity (r_2) values as compared to commercial T2 contrast agents. Similarly, near-infrared (NIR) two-photon

fluorescence emitting Fe_3O_4 nanostructures are prepared through trimesic acid/citrate-mediated reaction process for live cell multimodal imaging (Liao et al. 2013). In another study, SPIONs and IR-780 dye are co-encapsulated inside stearic acid-modified polyethylenimine to form a dual-modality contrast agent, which have effectively labeled and tracked the stem cells through MRI and near-infrared fluorescence (NIRF) imaging, respectively (Liu et al. 2016).

12.5.2 Thermo-chemotherapy

Thermo-chemotherapy that constitutes MFH therapy and chemotherapy is an effective dual/combined therapy used for cancer treatment, which is performed via SPION-based nano-carriers (SNCs, i.e., SPIONs are co-encapsulated along with chemotherapeutic drugs (CHDs) inside polymeric carrier/vehicles) (Hervault and Thanh 2014). Herein, MFH therapy is utilized to enhance the sensitivity of cancer cells toward CHDs, and this phenomenon is known as "chemo-sensitization" that occurs due to (1) increase in cell membrane permeability, and (2) reduction of the interstitial fluid pressure due to heating from MFH therapy (via SPIONs). Consequently, the uptake of the CHDs by the cancerous cells might significantly increase. Thus, thermo-chemotherapy is more effective to treat cancer than MFH alone. In addition, MRI could also be performed for simultaneous tumor imaging while performing thermo-chemotherapy due to the presence of SPIONs (contrast agent) (Rao et al. 2010; Li et al. 2018). Figure 12.10 represents the possible mechanism involved in cancer treatment via thermo-chemotherapy by using CHDs and SPIONs co-loaded SNCs.

In a recent investigation, the as-prepared 150-nm-sized magnetoliposomes, consisting of magnetite nanoparticle cores and the anticancer drug gemcitabine encapsulated by a phospholipid bilayer, have displayed 70% drug release and better elevated temperature—i.e., from 32 to 52 °C in 5 min—in time-dependent temperature curves, when exposed to AMF with H = 30 kA/m and f = 356 kHz (Ferreira et al. 2016). In another investigation, 370-nm-sized thermosensitive nanocomposites are prepared by having SPIONs/5-fluorouracil (anticancer drug) in the core and poly(*N*-isopropylacrylamide) (PNIPAM) polymer/silica (SiO_2) in the shell. These nanocomposites have displayed good thermal efficacy (rise to therapeutic temperature of 45 °C in 3.7 min) and faster drug release at relatively lower magnetic field (Shen et al. 2016). Moreover very recently, 64-nm-sized core-shell nanoparticles are prepared with tightly clustered Fe_3O_4 nanoparticles (having 17 nm size) in the core and doxorubicin (Dox—anticancer drug)-containing polymer in the shell (Hayashi et al. 2017). These nanoparticles have displayed a higher therapeutic efficacy against intraperitoneal tumors (located in BALB/c-nu/nu mice) via thermo-chemotherapy (i.e., MFH and chemotherapy) as compared to only thermotherapy (i.e., MFH) or chemotherapy alone. Herein, good heating efficacy (i.e., SAR values of 194–353 W/g) and faster drug release (49% in 20 min) under the influence of an

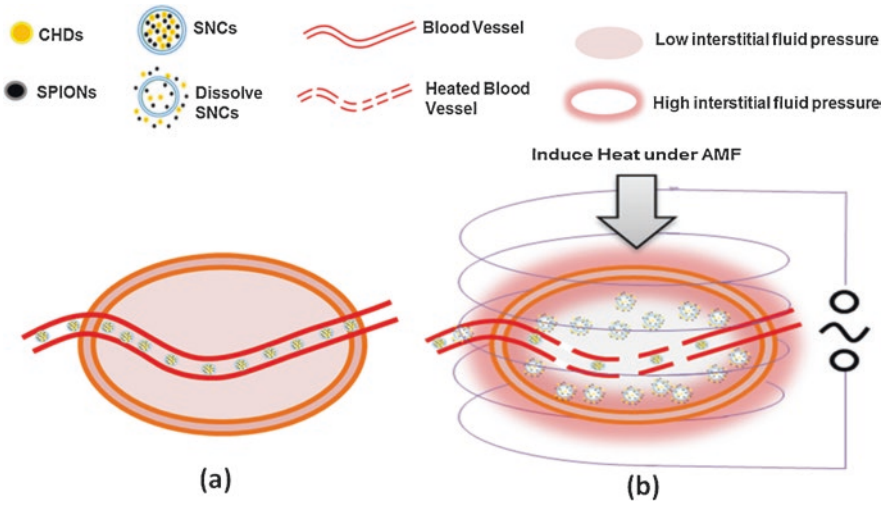

Fig. 12.10 Schematic representation of mechanism of the thermo-chemotherapy, (**a**) chemotherapy alone, and (**b**) thermo-chemotherapy (combined MFH and chemotherapy)

externally applied AMF (with $H = 8$ kA/m and $f = 217$ kHz) have resulted in the overall improvement of cancer therapeutic efficiency.

12.5.3 Thermo-radiotherapy

Thermo-radiotherapy that comprises MFH-based thermotherapy and radiation therapy/radiotherapy is another effective dual/combined therapy employed in cancer treatments, which is implemented via utilization of SPIONs (for MFH) and application of high-energy X-rays/gamma radiations (for radiotherapy). Generally in radiotherapy, high energy radiations destroy the cancer cells by damaging their genetic material (such as deoxyribonucleic acid (DNA)) either via direct interaction with cellular DNA, or interaction of free radicals (generated due to ionization/excitation of the water component) with DNA. Consequently, the shrinkage of tumor happens due to the death of cancerous cells through apoptosis, necrosis, mitotic catastrophe, or inhibition of the cell proliferation (Baskar et al. 2014; Desouky et al. 2015). However, the cancer cells may recover via (1) repairing their DNA damage, and (2) proliferation from their residual cells, after radiotherapy. Thus, the combined therapy might be preferred for the treatment of cancer to resolve this challenge. MFH can be effectively used as an adjuvant therapy for radiation therapy also, which might enhance the radio-sensitization effect in cancer cells or used to destroy the remaining cancer cells left after radiation therapy (Datta et al. 2015; Kaur et al. 2011). Besides, MRI can be combined with thermo-radiotherapy for effective tumor imaging also. For instance, in a study, the accumulation of gadolinium-doped iron

oxide nanoparticles (GdIONPs) in tumor region is clearly tracked and quantified by T2-weighted MRI (Jiang et al. 2017). Furthermore, these GdIONPs have displayed higher SAR value in time-dependent temperature/calorimetric studies and demonstrated high therapeutic efficacy in C57BL/6J mice with (TRAMP)-C1 prostate cancer, while used in combination with radiotherapy by utilizing a 25 Gy radiation therapy followed by a thermotherapy (via these nanoparticles and by applying AMF with $H = 19.57$ kA/m and $f = 52$ kHz) for 30 min. Moreover, the tumor growth curve has showed that the radiotherapy and thermotherapy have similar effects on tumor growth delay (2.5 and 4.5 days, respectively), while the tumor growth is delayed more than 10 days by the combined/thermo-radiotherapy. Moreover, clinical trials are performed in cancer-bearing patients, where the results have showed increased survival rates for patients who are treated with combined therapy/thermo-radiotherapy—mainly ascribed to the reduction in the actual radiation doses or the need for repeated radiotherapies (Maier-Hauff et al. 2011).

12.5.4 Thermo-immunotherapy

Now-a-days, immunotherapy has gained significant interest in cancer treatments, which is based on the killing of cancerous cells via artificial activation of immune system in human body. Usually, the cancer cells have antigens on their surface that act as a marker to reorganize and bind with the antibodies of the immune system, which may help in proliferation inhibition or killing of cancer cells (Farkona et al. 2016; Evans et al. 2018). The three prominent mechanisms that are involved in the cell death via immunotherapy include: (1) antibody-dependent cell-mediated cytotoxicity (ADCC) against tumor cells, which is triggered by the interaction of the fragment crystallizable (Fc) portion of the monoclonal antibodies (mAb) with the Fc receptors on the effector cells like natural killer cells, macrophages, and dendritic cells, (2) antibody-dependent cellular phagocytosis (ADCP), which is described as the target tumor cell elimination by the innate network of phagocytic cells, primarily neutrophils, monocytes, and macrophages, and (3) complement-dependent cytotoxicity, which is the result of the Fc region of an antigen–immunoglobulin complex triggering a cascade of more than 30 proteins that culminates in the formation of the membrane-attack complex, an amalgam of subunits that functions to perforate the phospholipid bilayer of the target cell and induce lysis (Jena 1997; Kohrt et al. 2015; Wang 2015). However, the delivery of antibodies alone to antigen-presenting cancer cells is insufficient to induce improved immunity due to their rapid degradation during the systemic administration. SPIONs can be used to improve the delivery of immunotherapeutic agents at the targeted tumor sites for enhanced cancer treatment via immunotherapy. For instance, the therapeutic efficacy of immunotherapy in FAT1-positive colorectal cancer is improved by magnetically targeting of the murine monoclonal antibodies (mAb198.3) conjugated SPIONs toward the cancer cells (Grifantini et al. 2018). Moreover, the activation of immune system against cancer can be done through heat stimulation via MFH by

using the SPIONs (Yanase et al. 1998; Toraya-Brown and Fiering 2014; Yagawa et al. 2017; Lin et al. 2018; Park et al. 2018).

12.6 Conclusions and Future Perspectives

In summary, nowadays new advancements are achieved in the synthesis of high-quality SPIONs using different synthesis routes in comparison to other types of magnetic nanoparticles, and also in the formation/stabilization of the ferrofluids (by using the SPIONs as major building blocks). Moreover, based on the abovementioned investigations, it can be clearly evident that the SPIONs have attained great importance in intrinsic cancer theranostics applications (such as MFH, MRI and magnetic drug delivery) and also in combined cancer theranostics applications (including MRI as an adjuvant to fluorescence imaging, thermo-chemotherapy, thermo-radiotherapy and thermo-immunotherapy). But, the overall utilization of the SPIONs is mainly restricted to in vitro levels. Nevertheless, very few high impacting efforts are being made to involve the SPIONs as an effective part of in vivo or clinical theranostics. For example, the global researchers have made worldwide consortiums that mainly focus to generate new treatment concepts (combined targeting radio-sensitization and thermotherapy via MFH), strengthen the existing synergies between technical advances, and inspect biocompatible coatings for magnetic nanoparticles (including SPIONs) in order to achieve breakthroughs in clinical cancer treatments. In addition, companies like "MagForce" (who developed ferrofluid and patented) have obtained FDA approval to conduct clinical studies by using "NanoTherm" for focal tumor ablation in prostate cancer with immediate risks. However, more fruitful attempts are needed so that, in near future the SPION-based theranostics will be used in full potential for treating the cancers effectively.

References

Abadeer NS, Murphy CJ. Recent progress in cancer thermal therapy using gold nanoparticles. J Phys Chem C. 2016;120(9):4691–716.

Ahn T, Kim JH, Yang HM, Lee JW, Kim JD. Formation pathways of magnetite nanoparticles by coprecipitation method. J Phys Chem C. 2012;116(10):6069–76.

Aires A, Ocampo SM, Simões BM, Josefa Rodríguez M, Cadenas JF, Couleaud P, Cortajarena AL. Multifunctionalized iron oxide nanoparticles for selective drug delivery to CD44-positive cancer cells. Nanotechnology. 2016;27(6):065103.

Ali A, Zafar H, Zia M, ul Haq I, Phull AR, Ali JS, Hussain A. Synthesis, characterization, applications, and challenges of iron oxide nanoparticles. Nanotechnol Sci Appl. 2016;9:49–67.

Ali LMA, Marzola P, Nicolato E, Fiorini S, De M. Polymer-coated superparamagnetic iron oxide nanoparticles as T2 contrast agent for MRI and their uptake in liver. Future Sci OA. 2017;5:FSO235.

Ansari MO, Ahmad MF, Shadab GGHA, Siddique HR. Superparamagnetic iron oxide nanoparticles based cancer theranostics: a double edge sword to fight against cancer. J Drug Deliv Sci Technol. 2018;45:177–83.

Araki EH, Ehlers J, Hepp K, Tvergaard JSV, Potier-ferry M. Colloidal magnetic fluids: basics, development and application of ferrofluid, Lecture notes in physics. Berlin: Springer Science & Business Media; 2009.

Arriortua OK, Garaio E, de la Parte BH, Insausti M, Lezama L, Plazaola F, et al. Antitumor magnetic hyperthermia induced by RGD-functionalized Fe3O4 nanoparticles, in an experimental model of colorectal liver metastases. Beilstein J Nanotechnol. 2016;7(1):1532–42.

Baskar R, Dai J, Wenlong N, Yeo R, Yeoh K-W. Biological response of cancer cells to radiation treatment. Front Mol Biosci. 2014;1:1–9.

Bastow TJ, Trinchi A. NMR analysis of ferromagnets: Fe oxides. Solid State Nucl Magn Reson. 2009;35(1):25–31.

Bedanta S, Kleemann W. Supermagnetism. J Phys D Appl Phys. 2009;42(1):013001.

Boutonnet M, Lögdberg S, Elm Svensson E. Recent developments in the application of nanoparticles prepared from w/o microemulsions in heterogeneous catalysis. Curr Opin Colloid Interface Sci. 2008;13(4):270–86.

Burgess A, Shah K, Hough O, Hynynen K. Next generation superparamagnetic iron oxide nanoparticles for cancer theranostics. Drug Discov Today. 2016;15(5):477–91.

Chopra M, Kandasamy G, Maity D. Multifunctional magnetic nanoparticles—a promising approach for cancer treatment. J Nanomed Res. 2016;4(1):3–4.

Cornell RM, Schwertmann U. Introduction to iron oxides. In: The iron oxides: structure, properties, reactions, occurences and uses. Weinheim: Wiley; 2004. p. 1–7. https://doi.org/10.1002/3527602097. ISBN: 9783527302741 (Print); 9783527602094 (Online).

Corot C, Warlin D. Superparamagnetic iron oxide nanoparticles for MRI: contrast media pharmaceutical company R&D perspective. Wiley Interdiscip Rev Nanomed Nanobiotechnol. 2013;5(5):411–22.

Danhier F, Feron O, Préat V. To exploit the tumor microenvironment: passive and active tumor targeting of nanocarriers for anti-cancer drug delivery. J Control Release. 2010;148(2):135–46.

Datta NR, Ordóñez SG, Gaipl US, Paulides MM, Crezee H, Gellermann J, et al. Local hyperthermia combined with radiotherapy and-/or chemotherapy: recent advances and promises for the future. Cancer Treat Rev. 2015;41(9):742–53.

Demirer GS, Okur AC, Kizilel S. Synthesis and design of biologically inspired biocompatible iron oxide nanoparticles for biomedical applications. J Mater Chem B. 2015;3(40):7831–49.

Desouky O, Ding N, Zhou G. Targeted and non-targeted effects of ionizing radiation. J Radiat Res Appl Sci. 2015;8(2):247–54.

Efremova MV, Naumenko VA, Spasova M, Garanina AS, Abakumov MA, Blokhina AD, et al. Magnetite-gold nanohybrids as ideal all-in-one platforms for theranostics. Sci Rep. 2018;8(1):1–19.

Evans ER, Bugga P, Asthana V, Drezek R. Metallic nanoparticles for cancer immunotherapy. Mater Today. 2018;21(6):673–85.

Farkona S, Diamandis EP, Blasutig IM. Cancer immunotherapy: the beginning of the end of cancer? BMC Med. 2016;14(1):1–18.

Fass L. Imaging and cancer: a review. Mol Oncol. 2008;2:115–52.

Ferreira RV, Martins TM, Goes AM, Fabris JD, Cavalcante LCD, Outon LEF, Domingues RZ. Thermosensitive gemcitabine-magnetoliposomes for combined hyperthermia and chemotherapy. Nanotechnology. 2016;27(8):085105.

Fu C, Ravindra NM. Magnetic iron oxide nanoparticles: synthesis and applications. Bioinspir Biomim Nanobiomater. 2012;1(4):229–44.

Ganipineni LP, Ucakar B, Joudiou N, Bianco J, Danhier P, Zhao M, et al. Magnetic targeting of paclitaxel-loaded poly(lactic-co-glycolic acid)-based nanoparticles for the treatment of glioblastoma. Int J Nanomed. 2018;13:4509–21.

Gilchrist RK, Medal R, Shorey WD, Hanselman RC, Parrott JC, Taylor CB. Selective inductive heating of lymph nodes. Ann Surg. 1957;146(4):596–606.

Gkanas EI. In vitro magnetic hyperthermia response of iron oxide MNP's incorporated in DA3, MCF-7 and HeLa cancer cell lines. Cent Eur J Chem. 2013;11(7):1042–54.

Grifantini R, Taranta M, Gherardini L, Naldi I, Parri M, Grandi A, Cinti C. Magnetically driven drug delivery systems improving targeted immunotherapy for colon-rectal cancer. J Control Release. 2018;280:76–86.

Grover VPB, Tognarelli JM, Crossey MME, Cox IJ, Taylor-Robinson SD, McPhail MJW. Magnetic resonance imaging: principles and techniques: lessons for clinicians. J Clin Exp Hepatol. 2015;5(3):246–55.

Gupta KM, Gupta N. Advanced electrical and electronics materials: processes and applications. Hoboken, NJ: Wiley; 2015.

Hairston RJ. The management of cytomegalovirus-associated retinal detachments. J Int Assoc Phys AIDS Care. 1996;2(5):31–4.

Hayashi K, Sato Y, Sakamoto W, Yogo T. Theranostic nanoparticles for MRI-guided thermochemotherapy: "tight" clustering of magnetic nanoparticles boosts relaxivity and heat-generation power. ACS Biomater Sci Eng. 2017;3(1):95–105.

Hervault A, Thanh NTK. Magnetic nanoparticle-based therapeutic agents for thermo-chemotherapy treatment of cancer. Nanoscale. 2014;6(20):11553–73.

Ibarra J, Encinas D, Blanco M, Barbosa S, Taboada P, Juárez J, Valdez MA. Co-encapsulation of magnetic nanoparticles and cisplatin within biocompatible polymers as multifunctional nanoplatforms: synthesis, characterization, and in vitro assays. Mater Res Express. 2018;5(1):015023.

Issa B, Obaidat IM, Albiss BA, Haik Y. Magnetic nanoparticles: surface effects and properties related to biomedicine applications. Int J Mol Sci. 2013;14(11):21266–305.

Ito A, Ito Y, Matsushima S, Tsuchida D, Ogasawara M, Hasegawa J, et al. New whole-body multimodality imaging of gastric cancer peritoneal metastasis combining fluorescence imaging with ICG-labeled antibody and MRI in mice. Gastric Cancer. 2014;17(3):497–507.

Jacques V, Dumas S, Sun W-C, Troughton J, Greenfield MT, Caravan P. High relaxivity MRI contrast agents part 2: optimization of inner- and second-sphere relaxivity. Investig Radiol. 2010;45(10):613–24.

Jena BP. Atomic force microscope: providing new insights on the structure and function of living cells. Cell Biol Int. 1997;21(11):683–4.

Jiang PS, Tsai HY, Drake P, Wang FN, Chiang CS. Gadolinium-doped iron oxide nanoparticles induced magnetic field hyperthermia combined with radiotherapy increases tumour response by vascular disruption and improved oxygenation. Int J Hyperth. 2017;33:1–9.

Jo SD, Ku SH, Won YY, Kim SH, Kwon IC. Targeted nanotheranostics for future personalized medicine: recent progress in cancer therapy. Theranostics. 2016;6:1362–77.

Josephson L, Kircher MF, Mahmood U, Tang Y, Weissleder R. Near-infrared fluorescent nanoparticles as combined MR/optical imaging probes. Bioconjug Chem. 2002;13(3):554–60.

Kalikmanov VI. Ferrofluids. In: Statistical physics of fluids Texts and Monographs in Physics. https://doi.org/10.1007/978-3-662-04536-7. Springer, Berlin, Heidelberg 2001. pp. 223–238.

Kandasamy G, Maity D. Recent advances in superparamagnetic iron oxide nanoparticles (SPIONs) for in vitro and in vivo cancer nanotheranostics. Int J Pharm. 2015;496(2):191–218.

Kandasamy G, Sudame A, Bhati P, Chakrabarty A, Maity D. Systematic investigations on heating effects of carboxyl-amine functionalized superparamagnetic iron oxide nanoparticles (SPIONs) based ferrofluids for in vitro cancer hyperthermia therapy. J Mol Liq. 2018a;256:224–37.

Kandasamy G, Sudame A, Luthra T, Saini K, Maity D. Functionalized hydrophilic superparamagnetic iron oxide nanoparticles for magnetic fluid hyperthermia application in liver cancer treatment. ACS Omega. 2018b;3(4):3991–4005.

Kandasamy G, Khan S, Giri J, Bose S, Veerapu NS, Maity D. One-pot synthesis of hydrophilic flower-shaped iron oxide nanoclusters (IONCs) based ferrofluids for magnetic fluid hyperthermia applications. J Mol Liq. 2019a;275:699–712.

Kandasamy G, Soni S, Sushmita K, Veerapu NS, Bose S, Maity D. One-step synthesis of hydrophilic functionalized and cytocompatible superparamagnetic iron oxide nanoparticles (SPIONs) based aqueous ferrofluids for biomedical applications. J Mol Liq. 2019b;274:653–63.

Kaur P, Hurwitz MD, Krishnan S, Asea A. Combined hyperthermia and radiotherapy for the treatment of cancer. Cancers. 2011;3(4):3799–823.

Kim DH, Vitol EA, Liu J, Balasubramanian S, Gosztola DJ, Cohen EE, et al. Stimuli-responsive magnetic nanomicelles as multifunctional heat and cargo delivery vehicles. Langmuir. 2013;29(24):7425–32.

Kitture R, Ghosh S, Kulkarni P, Liu XL, Maity D, Patil SI, et al. Fe3O4-citrate-curcumin: promising conjugates for superoxide scavenging, tumor suppression and cancer hyperthermia. J Appl Phys. 2012;111(6):064702.

Kohrt H, Rajasekaran N, Chester C, Yonezawa A, Zhao X. Enhancement of antibody-dependent cell mediated cytotoxicity: a new era in cancer treatment. Immunotargets Ther. 2015;4:91.

Kokura S, Yoshikawa T, Ohnishi T. Hyperthermic oncology from bench to bedside. Singapore: Springer; 2016.

Kosaka N, Ogawa M, Choyke PPL, Kobayashi H. Clinical implications of near-infrared fluorescence imaging in cancer. Future Oncol. 2009;5(9):1501–11.

Kozissnik B, Bohorquez AC, Dobson J, Rinaldi C. Magnetic fluid hyperthermia: advances, challenges, and opportunity. Int J Hyperth. 2013;29(8):706–14.

Kudr J, Haddad Y, Richtera L, Heger Z, Cernak M, Adam V, Zitka O. Magnetic nanoparticles: from design and synthesis to real world applications. Nanomaterials. 2017;7(9):243.

Kumar CSSR, Leuschner C. Nanoparticles for cancer drug delivery. In: Nanofabrication towards biomedical applications: techniques, tools, applications, and impact. Weinheim: Wiley-VCH; 2005.

Lahiri BB, Muthukumaran T, Philip J. Magnetic hyperthermia in phosphate coated iron oxide nanofluids. J Magn Magn Mater. 2016;407:101–13.

Laurent S, Forge D, Port M, Roch A, Robic C, Vander Elst L, Muller RN. Magnetic iron oxide nanoparticles: synthesis, stabilization, vectorization, physicochemical characterizations and biological applications. Chem Rev. 2008;108(6):2064–110.

Laurent S, Dutz S, Häfeli UO, Mahmoudi M. Magnetic fluid hyperthermia: focus on superparamagnetic iron oxide nanoparticles. Adv Colloid Interf Sci. 2011;166(1–2):8–23.

Laurent S, Saei AA, Behzadi S, Panahifar A, Mahmoudi M. Superparamagnetic iron oxide nanoparticles for delivery of therapeutic agents: opportunities and challenges. Expert Opin Drug Deliv. 2014;11(9):1449–70.

Li W, Hinton CH, Lee SS, Wu J, Fortner JD. Surface engineering superparamagnetic nanoparticles for aqueous applications: design and characterization of tailored organic bilayers. Environ Sci Nano. 2015;3:1–20.

Li X, Wei J, Aifantis KE, Fan Y, Feng Q, Cui FZ, Watari F. Current investigations into magnetic nanoparticles for biomedical applications. J Biomed Mater Res A. 2016;104:1285–96.

Li Q, Kartikowati CW, Horie S, Ogi T, Iwaki T, Okuyama K. Correlation between particle size/domain structure and magnetic properties of highly crystalline Fe3O4 nanoparticles. Sci Rep. 2017;7(1):1–4.

Li M, Bu W, Ren J, Li J, Deng L, Gao M, et al. Enhanced synergism of thermo-chemotherapy for liver cancer with magnetothermally responsive nanocarriers. Theranostics. 2018;8(3):693–709.

Liao MY, Wu CH, Lai PS, Yu J, Lin HP, Liu TM, Huang CC. Surface state mediated NIR two-photon fluorescence of iron oxides for nonlinear optical microscopy. Adv Funct Mater. 2013;23:2044–51.

Lin BL, Zhang JZ, Lu LJ, Mao JJ, Cao MH, Mao XH, Shen J. Superparamagnetic iron oxide nanoparticles-complexed cationic amylose for in vivo magnetic resonance imaging tracking of transplanted stem cells in stroke. Nanomaterials. 2017;7(5):107.

Lin FC, Hsu CH, Lin YY. Nano-therapeutic cancer immunotherapy using hyperthermia-induced heat shock proteins: insights from mathematical modeling. Int J Nanomed. 2018;13:3529–39.

Liu S, Jia B, Qiao R, Yang Z, Yu Z, Liu Z, et al. A novel type of dual-modality molecular probe for MR and nuclear imaging of tumor: preparation, characterization and in vivo application. Mol Pharm. 2009;6(4):1074–82.

Liu H, Tan Y, Xie L, Yang L, Zhao J, Bai J, et al. Self-assembled dual-modality contrast agents for non-invasive stem cell tracking via near-infrared fluorescence and magnetic resonance imaging. J Colloid Interface Sci. 2016;478:217–26.

Mahmoudi M, Sant S, Wang B, Laurent S, Sen T. Superparamagnetic iron oxide nanoparticles (SPIONs): development, surface modification and applications in chemotherapy. Adv Drug Deliv Rev. 2011;63(1–2):24–46.

Maier-Hauff K, Ulrich F, Nestler D, Niehoff H, Wust P, Thiesen B, et al. Efficacy and safety of intratumoral thermotherapy using magnetic iron-oxide nanoparticles combined with external beam radiotherapy on patients with recurrent glioblastoma multiforme. J Neurooncol. 2011;103(2):317–24.

Maity D, Agrawal DC. Synthesis of iron oxide nanoparticles under oxidizing environment and their stabilization in aqueous and non-aqueous media. J Magn Magn Mater. 2007;308(1):46–55.

Maity D, Ding J, Xue JM. Synthesis of magnetite nanoparticles by thermal decomposition: time, temperature, surfactant and solvent effects. Funct Mater Lett. 2008;01(3):189–93.

Maity D, Ding J, Xue JM. One-pot synthesis of hydrophilic and hydrophobic ferrofluid. Int J Nanosci. 2009;8(1–2):65–9.

Maity D, Chandrasekharan P, Si-Shen F, Xue JM, Ding J. Polyol-based synthesis of hydrophilic magnetite nanoparticles. J Appl Phys. 2010a;107(9):09B310.

Maity D, Chandrasekharan P, Yang CT, Chuang KH, Shuter B, Xue JM, Feng SS. Facile synthesis of water-stable magnetite nanoparticles for clinical MRI and magnetic hyperthermia applications. Nanomedicine. 2010b;5(10):1571–84.

Maity D, Chandrasekharan P, Pradhan P, Chuang K-H, Xue J-M, Feng S-S, Ding J. Novel synthesis of superparamagnetic magnetite nanoclusters for biomedical applications. J Mater Chem. 2011a;21(38):14717.

Maity D, Pradhan P, Chandrasekharan P, Kale SN, Shuter B, Bahadur D, Ding J. Synthesis of hydrophilic superparamagnetic magnetite nanoparticles via thermal decomposition of Fe(acac)3 in 80 Vol% TREG + 20 Vol% TREM. J Nanosci Nanotechnol. 2011b;11(3):2730–4.

Maxwell DJ, Bonde J, Hess DA, Hohm SA, Lahey R, Zhou P, et al. Fluorophore-conjugated iron oxide nanoparticle labeling and analysis of engrafting human hematopoietic stem cells. Stem Cells. 2008;26(2):517–24.

McCarthy MJ. Introduction to magnetic resonance imaging (MRI). In: Magnetic resonance imaging in foods; 2011. pp. 1–29.

Mclaughlin R, Hylton N, Imaging B. MRI in breast cancer therapy monitoring. NMR Biomed. 2015;24(6):712–20.

Merbach A, Helm L, Tóth É. The chemistry of contrast agents in medical magnetic resonance imaging. 2nd ed. Oxford: Wiley-Blackwell; 2013.

Mishra SK, Kumar BSH, Khushu S, Tripathi RP, Gangenahalli G. Increased transverse relaxivity in ultrasmall superparamagnetic iron oxide nanoparticles used as MRI contrast agent for biomedical imaging. Contrast Media Mol Imaging. 2016;11(5):350–61.

Mojica Pisciotti ML, Lima E, Vasquez Mansilla M, Tognoli VE, Troiani HE, Pasa AA, Zysler RD. In vitro and in vivo experiments with iron oxide nanoparticles functionalized with dextran or polyethylene glycol for medical applications: magnetic targeting. J Biomed Mater Res B Appl Biomater. 2014;102(4):860–8.

Morel A, Nikitenko SI, Gionnet K, Wattiaux A, Lai-kee-him J, Labrugere C, Faculte A. Sonochemical approach to the synthesis of Fe_3O_4@SiO_2 core–shell nanoparticles with tunable properties. ACS Nano. 2008;2(5):847–56.

Moskowitz BM. Hitchhiker's guide to magnetism. Environmental magnetism workshop, vol. 279(1), 1991. p. 48.

Mutin PH, Vioux A. Nonhydrolytic processing of oxide-based materials: simple routes to control homogeneity, morphology, and nanostructure. Chem Mater. 2009;21(4):582–96.

Nitz WR, Reimer P. Contrast mechanisms in MR imaging. Eur Radiol. 1999;9(6):1032–46.
Odenbach S. Ferrofluids—magnetically controllable fluids and their applications. Berlin: Springer; 2002.
Odenbach S. Ferrofluids—magnetically controlled suspensions. Colloids Surf A Physicochem Eng Asp. 2003;217(1–3):171–8.
Ohno T, Wakabayashi T, Takemura A, Yoshida J, Ito A, Shinkai M, Kobayashi T. Effective solitary hyperthermia treatment of malignant glioma using stick type CMC-magnetite. In vivo study. J Neurooncol. 2002;56(3):233–9.
Okoli C, Boutonnet M, Mariey L, Jaras S, Rajarao G. Application of magnetic iron oxide nanoparticles prepared from microemulsions for protein purification. J Chem Technol Biotechnol. 2011;86(11):1386–93.
Ortega RA, Giorgio TD. A mathematical model of superparamagnetic iron oxide nanoparticle magnetic behavior to guide the design of novel nanomaterials. J Nanopart Res. 2012;14(12):1282.
Park W, Heo Y-J, Han DK. New opportunities for nanoparticles in cancer immunotherapy. Biomater Res. 2018;22(1):24.
Piñeiro Y, Vargas Z, Rivas J, Lõpez-Quintela MA. Iron oxide based nanoparticles for magnetic hyperthermia strategies in biological applications. Eur J Inorg Chem. 2015;2015(27):4495–509.
Pinkas J, Reichlova V, Zboril R, Moravec Z, Bezdicka P, Matejkova J. Sonochemical synthesis of amorphous nanoscopic iron(III) oxide from Fe(acac)3. Ultrason Sonochem. 2008;15(3):257–64.
Polyak B, Friedman G. Magnetic targeting for site-specific drug delivery: applications and clinical potential. Expert Opin Drug Deliv. 2009;6(1):53–70.
Pooley R. Fundamental Physics of MR Imaging. Radiographics. 2005;25(4):1087–99.
Prashant C, Dipak M, Yang CT, Chuang KH, Jun D, Feng SS. Superparamagnetic iron oxide—loaded poly (lactic acid)-d-alpha-tocopherol polyethylene glycol 1000 succinate copolymer nanoparticles as MRI contrast agent. Biomaterials. 2010;31(21):5588–97.
Prijic S, Sersa G. Magnetic nanoparticles as targeted delivery systems in oncology. Radiol Oncol. 2011;45(1):1–16.
Qiao R, Yang C, Gao M. Superparamagnetic iron oxide nanoparticles: from preparations to in vivo MRI applications. J Mater Chem. 2009;19(35):6274.
Rabias I, Tsitrouli D, Karakosta E, Kehagias T, Diamantopoulos G, Fardis M, Papavassiliou G. Rapid magnetic heating treatment by highly charged maghemite nanoparticles on Wistar rats exocranial glioma tumors at microliter volume. Biomicrofluidics. 2010;4(2):024111.
Raj K, Boulton RJ. Ferrofluids—properties and applications. Mater Des. 1987;8(4):233–6.
Raj K, Moskowitz B, Casciari R. Advances in ferrofluid technology. J Magn Magn Mater. 1995;149(1–2):174–80.
Rao W, Deng ZS, Liu J. A review of hyperthermia combined with radiotherapy/chemotherapy on malignant tumors. Crit Rev Biomed Eng. 2010;38(1):101–16.
Revia RA, Zhang M. Magnetite nanoparticles for cancer diagnosis, treatment, and treatment monitoring: recent advances. Mater Today. 2016;19(3):157–68.
Rosenblum D, Joshi N, Tao W, Karp JM, Peer D. Progress and challenges towards targeted delivery of cancer therapeutics. Nat Commun. 2018;9(1):1410.
Rosensweig RE. Ferrohydrodynamics. Mineola: Dover Publications; 1997.
Scherer C, Neto AMF. Ferrofluids: properties and applications. Braz J Phys. 2005;35(3):718–27.
Schleich N, Po C, Jacobs D, Ucakar B, Gallez B, Danhier F, Préat V. Comparison of active, passive and magnetic targeting to tumors of multifunctional paclitaxel/SPIO-loaded nanoparticles for tumor imaging and therapy. J Control Release. 2014;194:82–91.
Shen B, Ma Y, Yu S, Ji C. Smart multifunctional magnetic nanoparticle-based drug delivery system for cancer thermo-chemotherapy and intracellular imaging. ACS Appl Mater Interfaces. 2016;8(37):24502–8.
Shen Z, Wu A, Chen X. Iron oxide nanoparticle based contrast agents for magnetic resonance imaging. Mol Pharm. 2017;14(5):1352–64.
Shin TH, Choi Y, Kim S, Cheon J. Recent advances in magnetic nanoparticle-based multi-modal imaging. Chem Soc Rev. 2015;44(14):4501–16.

Silva AC, Oliveira TR, Mamani JB, Malheiros SMF, Malavolta L, Pavon LF, Gamarra LF. Application of hyperthermia induced by superparamagnetic iron oxide nanoparticles in glioma treatment. Int J Nanomed. 2011;6:591–603.

Spaldin N. Magnetic materials-fundamentals and applications. Cambridge: Cambridge University Press; 2003.

Stephen ZR, Kievit FM, Zhang M. Magnetite nanoparticles for medical MR imaging. Mater Today. 2012;14(11):330–8.

Suto M, Hirota Y, Mamiya H, Fujita A, Kasuya R, Tohji K, Jeyadevan B. Heat dissipation mechanism of magnetite nanoparticles in magnetic fluid hyperthermia. J Magn Magn Mater. 2009;321(10):1493–6.

Tan YF, Chandrasekharan P, Maity D, Yong CX, Chuang KH, Zhao Y, Feng SS. Multimodal tumor imaging by iron oxides and quantum dots formulated in poly (lactic acid)-d-alpha-tocopheryl polyethylene glycol 1000 succinate nanoparticles. Biomaterials. 2011;32(11):2969–78.

Tartaj P, Del M, Morales P, Veintemillas-Verdaguer S, González-Carr T, Serna CJ. The preparation of magnetic nanoparticles for applications in biomedicine. J Phys D Appl Phys. 2003;36(36):182–97.

Thanh NTK. Magnetic nanoparticles: from fabrication to clinical applications. Boca Raton, FL: CRC Press; 2012.

Thanh NTK. Clinical applications of magnetic nanoparticles, vol. 91. Boca Raton, FL: CRC Press; 2018.

Thomsen LB, Thomsen MS, Moos T. Targeted drug delivery to the brain using magnetic nanoparticles. Ther Deliv. 2015;6(10):1145–55.

Toraya-Brown S, Fiering S. Local tumour hyperthermia as immunotherapy for metastatic cancer. Int J Hyperth. 2014;30(8):531–9.

Trohidou K, editor. Magnetic nanoparticle assemblies. Singapore: Pan Stanford Publishing; 2014.

Turcheniuk K, Tarasevych AV, Kukhar VP, Boukherroub R, Szunerits S. Recent advances in surface chemistry strategies for the fabrication of functional iron oxide based magnetic nanoparticles. Nanoscale. 2013;5(22):10729.

Veiseh O, Gunn J, Zhang M. Design and fabrication of magnetic nanoparticles for targeted drug delivery and imaging. Adv Drug Deliv Rev. 2011;62(3):284–304.

Wang W. NK cell-mediated antibody-dependent cellular cytotoxicity in cancer immunotherapy. Front Immunol. 2015;6(11):683–4.

Wang YJ, Xuan S, Port M, Idee J. Recent advances in superparamagnetic iron oxide nanoparticles for cellular imaging and targeted therapy research. Curr Pharm Des. 2013;19:6575–93.

Wei H, Bruns OT, Kaul MG, Hansen EC, Barch M, Wiśniowska A, et al. Exceedingly small iron oxide nanoparticles as positive MRI contrast agents. Proc Natl Acad Sci. 2017;114(9):2325–30.

Wu W, He Q, Jiang C. Magnetic iron oxide nanoparticles: synthesis and surface functionalization strategies. Nanoscale Res Lett. 2008;3(11):397–415.

Wu W, Wu Z, Yu T, Jiang C, Kim W-S. Recent progress on magnetic iron oxide nanoparticles: synthesis, surface functional strategies and biomedical applications. Sci Technol Adv Mater. 2015;16(2):023501.

Wu F, Su H, Zhu X, Wang K, Zhang Z, Wong WK. Near-infrared emissive lanthanide hybridized carbon quantum dots for bioimaging applications. J Mater Chem B. 2016;4(38):6366–72.

Xu C, Sun S. New forms of superparamagnetic nanoparticles for biomedical applications. Adv Drug Deliv Rev. 2013;65:732–43.

Yagawa Y, Tanigawa K, Kobayashi Y, Yamamoto M. Cancer immunity and therapy using hyperthermia with immunotherapy, radiotherapy, chemotherapy, and surgery. J Cancer Metastasis Treat. 2017;3(10):218.

Yanase M, Shinkai M, Honda H, Wakabayashi T, Yoshida J, Kobayashi T. Antitumor immunity induction by intracellular hyperthermia using magnetite cationic liposomes. Jpn J Cancer Res. 1998;89(7):775–82.

Yin X, Zhang J, Wang X. Sequential injection analysis system for the determination of arsenic by hydride generation atomic absorption spectrometry. Fenxi Huaxue. 2004;32(10):1365–7.

Yoffe S, Leshuk T, Everett P, Gu F. Superparamagnetic iron oxide nanoparticles (SPIONs): synthesis and surface modification techniques for use with MRI and other biomedical applications. Curr Pharm Des. 2013;19:493–509.

Yu MK, Park J, Jon S. Targeting strategies for multifunctional nanoparticles in cancer imaging and therapy. Theranostics. 2012;2(1):3–44.

Zhang Y, Zhang B, Liu F, Luo J, Bai J. In vivo tomographic imaging with fluorescence and MRI using tumor-targeted dual-labeled nanoparticles. Int J Nanomed. 2013;9(1):33–41.

Zhu L, Zhou Z, Mao H, Yang L. Magnetic nanoparticles for precision oncology: theranostic magnetic iron oxide nanoparticles for image-guided and targeted cancer therapy. Nanomedicine. 2017;12(1):73–87.